Letter

Importance of gyrokinetic exact Fokker-Planck collisions in fusion plasma turbulence

Qingjiang Pan [*] and Darin R. Ernst [†]
Plasma Science and Fusion Center, Massachusetts Institute of Technology, Cambridge, Massachusetts 02139, USA

David R. Hatch
Institute for Fusion Studies, University of Texas at Austin, Austin, Texas 78712, USA

(Received 15 December 2019; revised 20 October 2020; accepted 13 April 2021; published 17 May 2021)

Gyrokinetic simulations of turbulence are fundamental to understanding and predicting particle and energy loss in magnetic fusion devices. Previous works have used model collision operators with approximate field-particle terms of unknown accuracy and/or have neglected collisional finite Larmor radius effects. This work moves beyond models to demonstrate important corrections using a gyrokinetic Fokker-Planck collision operator with the exact field-particle terms, in realistic simulations of turbulence in magnetically confined fusion plasmas. The exact operator shows significant corrections for temperature-gradient-driven trapped electron mode turbulence and zonal flow damping, and for microtearing modes in a Joint European Torus pedestal under ITER-like wall conditions. Analysis of the corrections using parameter scans motivates an accurate model which closely reproduces the exact results while reducing computational demands.

DOI: 10.1103/PhysRevE.103.L051202

Introduction. Gyrokinetic simulations of turbulence are routinely performed to understand and predict the confinement of magnetic fusion devices. The turbulence responsible for most particle and energy loss in fusion devices has eddy sizes at the scales of particle gyroradii. Gyrokinetic simulations of this microscale turbulence solve the gyrokinetic equation obtained by averaging the Fokker-Planck kinetic equation over the very high frequency particle gyromotion, while retaining finite Larmor radius (FLR) effects [1].

Fusion plasma turbulence can be sensitive to particle collisions. Previous gyrokinetic turbulence simulations have used only approximate collision operators, where simplified moment models replace the exact Fokker-Planck field-particle terms and/or FLR terms are neglected altogether (see Ref. [2] for a brief summary of collisions used in gyrokinetic simulations). The state-of-the-art Sugama collision model [3], recently implemented in the gyrokinetic GKV [4], CGYRO [5], and GENE [6] codes, extends the like-species Abel model [7,8] to include collisions between unlike species with unequal temperatures, while preserving the self-adjointness and Boltzmann's H–theorem. For equal-temperature cases considered in this Letter, the test-particle part of these models is exact (i.e., identical to the linearized Fokker-Planck counterpart), but the back-reaction field-particle part is modeled with two terms restoring overall momentum and energy conservation. When compared with the exact linearized Fokker-Planck operator, (1) the Abel model (without gyroaverage) yields 50% higher classical collisional ion thermal transport [8], and (2) the Abel and various collision models in the drift-kinetic limit (i.e., without FLR effects) are inaccurate for neoclassical transport and bootstrap current, as summarized in Ref. [9]. This motivates us to examine the accuracy of present collision models for gyrokinetic simulations and predictions of turbulent transport.

To this end, we have developed a gyrokinetic (i.e., including FLR effects) exact linearized Fokker-Planck collision operator [2] in the widely used gyrokinetic GENE code [10,11]. This operator formulation, referred to hereafter as the "exact" or "gyrokinetic exact" operator, automatically conserves particles, parallel momentum, and energy, and satisfies the H–theorem. Further, the conservation and H–theorem are preserved by using the conservative linearized Landau form [9], which, unlike the Rosenbluth form [12], explicitly preserves the symmetry between test- and field-particle contributions; numerical errors in the test-particle part are canceled by opposite errors in the field-particle part, retaining conservation independent of numerical resolution. The implementation applies a finite-volume method originally designed for a nonlinear drift-kinetic Fokker-Planck operator [13], and the method was adapted to implement the Sugama model in the GENE code [6]. Using the same numerical method as a basis for the gyrokinetic exact operator enables direct comparison with the Sugama model in the same code. In addition to the verification presented in Ref. [2], a direct cross-code benchmark in the drift-kinetic limit shows the exact and Sugama operators in GENE closely agree with their counterparts implemented in the NEO code [14] for neoclassical transport. Here, we show important corrections relative to the Sugama model for instabilities and turbulence that are relevant to fusion experiments.

Impact on TEM instability and turbulence. We first focus on trapped electron modes (TEMs), which are particularly sensitive to collisions, which detrap particles. TEMs are important in fusion plasmas with strong electron heating [15] as expected in burning plasmas which are self-heated

[*] panqj@psfc.mit.edu
[†] dernst@psfc.mit.edu

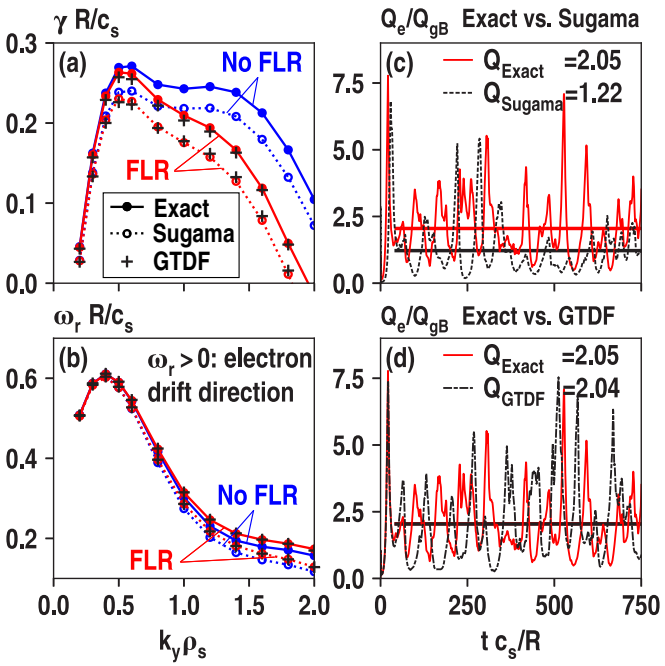

FIG. 1. Gyrokinetic simulations of TEM linear growth rates and nonlinear electron heat fluxes for $\eta_e = 1$. (a) Growth rates and (b) frequencies given by the exact operator (solid), the Sugama model (dotted), and the proposed GTDF model (pluses); (c) electron heat fluxes (normalized to gyroBohm) of the exact operator and the Sugama model; and (d) flux comparison of the exact operator with its GTDF model. In (a) and (b), the red (blue) lines are for cases with (without) FLR effects, and the exact and Sugama GTDF data are overlaid on their respective full-operator (i.e., with FLR effects) data. The horizontal lines in (c) and (d) represent the mean values of the indicated intervals.

by fusion reactions. Figure 1 presents TEM linear growth rates and frequencies from the eigenvalue solver and electron heat fluxes from nonlinear simulations, comparing the exact operator with the Sugama model. The parameters are from the cyclone case for an isothermal electron–deuterium plasma in a concentric circular geometry with safety factor $q = 1.4$, inverse aspect ratio $\varepsilon = r/R = 0.18$, and magnetic shear $s = (r/q)dq/dr = 0.796$, where r is the local minor radius and R is the major radius of the center of the cross section [16]. The gradients driving the turbulence, described by normalized inverse gradient scale lengths, are set to be $R/L_{n,T_e} = -R\,d\ln(n, T_e)/dr = 5$ (i.e., $\eta_e \equiv L_n/L_{T_e} = 1$), and the ion temperature gradient drive is set to zero. The normalized electron–ion collision frequency is set to be $\hat{\nu}_{ei} \equiv \nu_{ei}R/(\sqrt{2}c_s) = \sqrt{m_i/m_e}\pi e^4 n_e R \ln\Lambda/T_e^2 = 1$ with $c_s = \sqrt{T_e/m_i}$ and other quantities in standard notation, typical for the high density core of the Alcator C-Mod tokamak [17]. Linearly, the Sugama model captures the trend of the growth rate and frequency, and the larger reduction of growth rate by the collisional FLR effects at higher binormal wave number k_y [5,18], but broadly underestimates the growth rate. The relative difference of the peak growth rate is about 15%, occurring at $k_y\rho_s = 0.5 - 0.6$, with $\rho_s = c_s/\Omega_i$ and $\Omega_i = eB/m_i c$.

Nonlinearly, density-gradient-driven TEM turbulence onset occurs when the density gradient reaches a nonlinear critical value, which exceeds the linear critical value [17]. The gradient used in the present study is marginally above the nonlinear critical value where zonal flows regulate the turbulence and are damped by ion–ion collisions, a typical core operating point in experiments with strong electron heating [15]. The nonlinear fluxes shown in Fig. 1(c) are bursty with quasiperiodic oscillations which trade off between turbulent bursts and zonal flows and/or fields. We have varied the spatial domain size and resolution in additional nonlinear simulations with the Sugama operator and did not find meaningful changes in the fluxes. Despite the large fluctuations, the electron heat flux with the exact operator is systematically higher than the Sugama model by about 68% on average. The electron particle and thermal diffusivities using the exact operator are $D/D_{\rm gB} = 0.11$ and $\chi_e/\chi_{\rm gB} = 0.41$, where $D_{\rm gB} = \chi_{\rm gB} = c_s\rho_s^2/R$. These diffusivities are comparable to those obtained in Alcator C-Mod internal transport barrier (ITB) experiments [17]; using $T_e = 1$ keV, $B = 4.5$ T, and $R = 0.67$ m results in $\chi_e = 0.14$ m^2/s and $D = 0.038$ m^2/s, comparable with the experimentally inferred values.

Recall that the test-particle terms of the Sugama operator are exact, while the model field-particle terms differ from the exact ones, including the drift-kinetic part and the FLR part. To separate the two parts, calculations were made using the gyrokinetic test-particle and drift-kinetic field-particle (GTDF) terms of the exact operator. The results are shown in Figs. 1(a), 1(b), and 1(d). Interestingly, the GTDF model accurately captures the TEM eigenvalues, underestimating the peak growth rate by only about 2% as opposed to 15% for the Sugama model. Neglecting the field-particle FLR effects in the GTDF model yields a negligible difference in nonlinear electron heat flux. The field-particle FLR effects are negligible because they are higher order corrections to the field-particle terms, which are smaller than the test-particle terms [19]. Because the test-particle FLR corrections increase secularly with wave number, while the field-particle FLR corrections are associated with Bessel functions and decrease with wave number, the accuracy of the GTDF model should improve further with increasing wave number. As shown in Fig. 6 of Ref. [2] and Fig. 1(a) here, for the Sugama model the impact of the field-particle FLR effects on the growth rates is also minimal. To this order in gyroradius, neglecting the field-particle FLR terms does not break the *global* conservation laws, i.e., invariance of the velocity moments integrated over the entire phase space, because the FLR contributions to the moments can be written as a divergence of a collisional flux and are spatially averaged out [2].

Figure 2(a) shows a summary of the particle flux (normalized to $n_e c_s \rho_s^2/R^2$) and heat fluxes (normalized to $n_e T_e c_s \rho_s^2/R^2$) of both species. The electron heat transport is dominant, and the particle and ion heat transport are about four times smaller. Similar to the electron heat flux, the Sugama model underestimates the particle flux and ion heat flux. The GTDF model using the exact drift-kinetic field-particle terms is accurate for all nonlinear fluxes. Electron heat flux spectra as a function of k_y (not shown here) are also well described by the GTDF model. However, the exact operator produces higher and wider spectra than the Sugama model, resembling the broadly larger growth rate shown in Fig. 1(a).

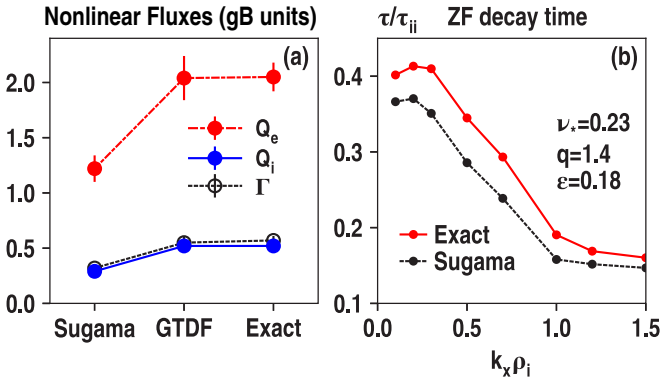

FIG. 2. (a) Summary of the mean nonlinear particle flux (Γ), and ion (Q_i) and electron (Q_e) heat fluxes in normalized units. The error bar indicates the standard deviation of the means of nonoverlapping windows based on autocorrelation time [20]. (b) Zonal flow decay time as a function of the radial wave number.

The spectra peak at $k_y\rho_s = 0.5$ for all three operators, close to where the growth rates peak.

Given the different TEM growth rates and turbulence fluctuation levels with the exact and Sugama collisions, the effects of zonal flow damping by the two operators on the fluxes cannot be directly compared in the nonlinear simulations. To isolate the zonal flow damping, we instead calculate the zonal flow decay time for the Hinton–Rosenbluth problem [21], in which a density perturbation is initialized at a single radial wave number and subsequently shielded by neoclassical polarization and damped by ion–ion collisions. The decay time is obtained by fitting the time trace of the flux-surface-averaged potential to a zonal flow decay model [2]. The result for both operators is summarized in Fig. 2(b). Here, the electrons are adiabatic and the same geometry as in the TEM case is used. The effective collision frequency for detrapping ions out of the magnetic well, normalized to the bounce frequency, is $\nu_* = 0.23$, corresponding to $\hat{\nu}_{ei} = 1$ as in the TEM case. The exact operator yields weaker zonal flow damping than the Sugama model by 10–20%. A weaker zonal flow damping tends to support a stronger zonal flow shear, hence weaker turbulence-induced transport. Thus the zonal flow damping channel counters the observed flux differences.

In contrast to the significant increases in TEM growth rate and nonlinear fluxes with the exact collision operator presented in this Letter, no appreciable differences in growth rate or fluxes were found in the density-gradient-driven TEM simulations in Ref. [2] (Fig. 4 therein), which used the same parameters except that the electron temperature gradient drive was absent there, i.e., $\eta_e = 0$. The TEMs in Fig. 1 here are partly driven unstable by the temperature gradient through wave-particle resonance with trapped electrons undergoing toroidal precession drift, in addition to the "fluidlike" interchange mechanism associated with the bad curvature in the outboard region that drives purely density-gradient-driven TEMs unstable (see Ref. [17] and references therein). The former mechanism relies on a small class of resonant trapped electrons and is apparently more sensitive to changes in the field-particle terms, which are nevertheless

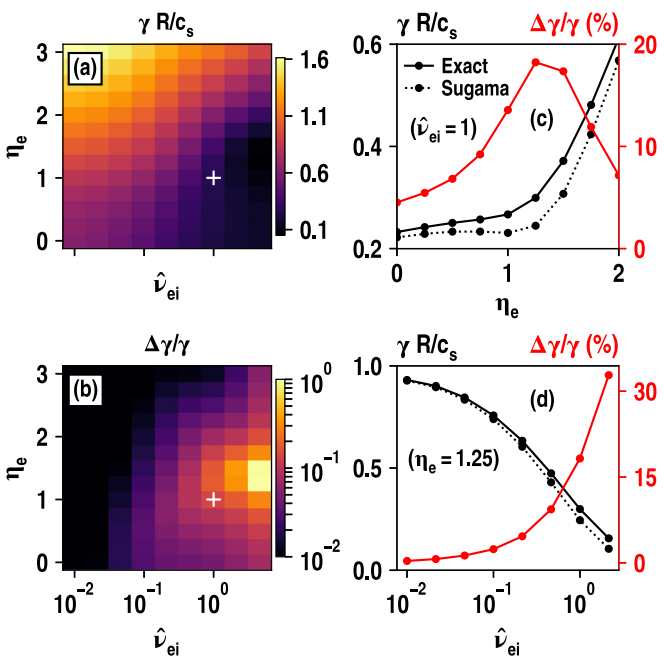

FIG. 3. Dependence of TEM growth rates on collisionality and η_e at fixed $k_y\rho_s = 0.5$ and $R/L_n = 5$. (a) Growth rates given by the exact operator, (b) relative difference of growth rates given by exact and Sugama operators, (c) growth rates and relative difference at $\hat{\nu}_{ei} = 1$, and (d) growth rates and relative difference at $\eta_e = 1.25$. The pluses in (a) and (b) indicate the parameters used in Fig. 1.

relatively small compared with pitch-angle scattering in the test-particle terms. However, the electron temperature gradient enters in proportion to the particle energy, so that its drive affects higher energies in the perturbed distribution and thus higher energy moments which are truncated by model field-particle operators [19]. As shown in Fig. 3, the relative difference in growth rate is minimal at $\eta_e = 0$, increases with η_e until it peaks at $\eta_e \simeq 1.25$, then drops with η_e. The absolute difference exhibits a similar trend (not shown here). When $\eta_e \gtrsim 1.25$, the instability continuously extends to the electron-temperature-gradient (ETG) instability regime at higher k_y and the "valley" at the intermediate k_y as shown in Fig. 6 of Ref. [2] disappears, indicating a change of mode character. The difference shown in Fig. 3 increases with collisionality.

Impact on microtearing mode instability. Microtearing modes (MTMs) are a type of dissipative electromagnetic modes that are typically destabilized by the electron temperature gradient through electron collisions; electron streaming along the perturbed magnetic field lines (magnetic flutter effect) feeds the tearing modes free energy and can drive experimentally relevant thermal transport in tokamaks [22–26]. To evaluate impact of the collision operators on MTMs with realistic parameters, we focus on the Joint European Torus (JET) pulse 82585 under ITER-like wall conditions; this shot is part of an experimental campaign studying the effects of deuterium fueling on pedestal structure [27]. Careful analyses of extensive GENE simulations by Hatch *et al.* [25] have identified the dominant unstable mode across most pedestal to be the MTM, using characteristics such as tearing parity of mode structures, negative (electron direction) mode frequencies, and

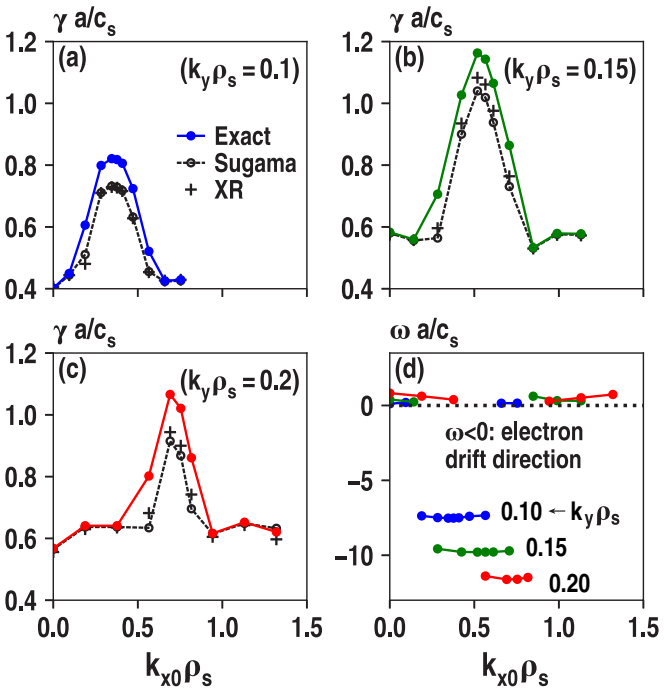

FIG. 4. Dependence in growth rates and frequencies vs central k_x at $\rho_{\rm tor} = 0.98$, comparing the exact operator (colored) with the Sugama (dashed) and Xu–Rosenbluth (XR) (crosses) models. Growth rates at (a) $k_y\rho_s = 0.1$, (b) $k_y\rho_s = 0.15$, and (c) $k_y\rho_s = 0.2$; (d) frequencies shown in blue, green, and red colors, corresponding to the three binormal wave numbers shown in (a), (b), and (c), respectively.

the magnetic component of fluctuations being essential for transport.

Figure 4 compares growth rates of the dominant modes given by the exact and Sugama operators in the steep gradient region at $\rho_{\rm tor} = 0.98$, where $\rho_{\rm tor}$ is the square root of the normalized toroidal magnetic flux. For reference, the parameters are $q = 3.9$, $s = 1.1$, $a/L_n = 18.1$, $\eta_e = \eta_i = 2.9$, $\hat{\nu}_{ei} = 6.1$, $\beta_e = 8\pi n_e T_e/B^2 = 1.2 \times 10^{-3}$, and $R/a = 2.48$, where R and a are the major and minor radii of the last-closed flux surface. An important feature of this pedestal MTM case is that it is most unstable at finite radial wave number k_x, which amounts to a shift in the ballooning angle in ballooning theory; the eigenmode peaks at the top and bottom of the tokamak. The exact collision operator does not alter this character, but yields appreciably larger growth rates than the Sugama model. The differences in the peak growth rate at $k_y\rho_s = 0.1$, 0.15, 0.2 are 10.8%, 10.8%, and 14.9%, respectively. Extensive convergence tests by varying resolution in each direction verified that these differences are physical. For comparison, the growth rates of the Xu–Rosenbluth gyrokinetic collision model [28] used by Hatch *et al.* [25] are also shown in Fig. 4. Like the Sugama operator, the Xu–Rosenbluth operator consists of exact test-particle terms and conserving model field-particle terms; however, the Xu–Rosenbluth field-particle model is not constructed to preserve the H–theorem. The peak growth rates given by the Xu–Rosenbluth model are slightly higher than the Sugama model at $k_y\rho_s = 0.15$ and $k_y\rho_s = 0.2$, but the discrepancy with the exact operator is significant. Notably, the growth rate discrepancy disappears where the dominant mode switches to drift-type modes with positive (ion direction) frequencies at the extremes of the k_{x0} range, which in contrast reveals that electron collisions sensitive to the changes in field-particle terms underlie the MTM corrections. Hatch *et al.* [25] suggested the temperature gradient drive in this case is well above the nonlinear critical gradient of the MTM; thus a standard quasilinear estimate suggests the larger growth rates would yield a 10–15% increase in transport [29]. As a result of "profile stiffness" and the known sensitivity of core to pedestal that it produces, this correction in the pedestal could be amplified in core confinement predictions. Further, turbulent transport can flatten the electron temperature profile and push the JET pedestal (with a carbon wall) to operate near a marginally unstable regime [30]. In such cases the exact and model operators can potentially predict substantially different pedestal transport. Due to strong shaping and extension of the unstable mode to higher k_y, nonlinear simulations of MTMs with the exact operator demand much more computational resources than the nonlinear TEM cases and are left for future work.

Conclusions. The parameter-dependent importance of the gyrokinetic exact Fokker-Planck collisions is reported for TEM and MTM cases that are relevant to tokamak fusion experiments in the core and pedestal, respectively. The exact operator and the recent and widely used Sugama model are implemented with the same finite-volume method in the same code, allowing direct assessments of the model accuracy. For TEMs, (1) the exact operator yields larger growth rates overall relative to the Sugama model and the difference increases with collisionality and temperature gradient drive, reaching a maximum at finite $\eta_e \sim 1.25$ before ETG modes begin to dominate; (2) for an $\eta_e = 1$ drive marginally above the nonlinear threshold, the larger growth rate produces significant (68%) increases in nonlinear fluxes, despite a weaker zonal flow damping with the exact operator; and (3) the differences in growth rates and nonlinear fluxes can be attributed to the exact drift-kinetic field-particle terms (without FLR effects); thus the GTDF model consisting of gyrokinetic test-particle terms and drift-kinetic field-particle terms can be used to alleviate the computational challenge of the full exact operator while retaining accuracy. For the MTM in a representative JET pedestal under ITER-like wall conditions, the exact operator yields appreciably larger growth rates than both the widely used Sugama and Xu–Rosenbluth models in the steep gradient region. The growth rate discrepancy disappears when drift-type modes become dominant, again suggesting the MTM corrections are due to the effect of the exact field-particle terms on instabilities driven by the electron temperature gradient. In all cases so far the corrections due to the exact field-particle terms are associated with instabilities that are driven by the electron temperature gradient and sensitive to collisions.

The present Letter materially extends the comparison between the exact operator and the Sugama model initially reported in Ref. [2] in several ways. First, although the different TEM growth rates given by the two operators previously published in Figs. 5 and 6 of Ref. [2] suggest the importance of the new operator, these are linear results and do not directly predict transport fluxes. In this Letter we have shown

the evidence of a substantial increase of the TEM nonlinear electron heat flux using the exact operator, relative to the most accurate collision model presently implemented. Notably, this ∼68% increase shown in Fig. 1(c) is much larger than the ∼15% increase in the peak growth rate shown in Fig. 1(a). The maximum difference in the peak growth rate in Fig. 5(b) of Ref. [2] (fixing $\eta_e = 1$) is also ∼15%. From the standard quasilinear theory, one would incorrectly predict a flux increase on the level of ∼15% at most, which would be appreciable but modest. This shows the complex amplification effect near the instability nonlinear threshold, where the turbulence and zonal flows and/or fields trade off quasiperiodically, underscoring the necessity of the nonlinear simulations shown here. Ultimately, the fusion community cares about nonlinear fluxes, which measure transport and loss. Second, as remarked earlier, the ∼68% flux increase with an electron temperature gradient drive contrasts with the minimal flux change observed for the purely density-gradient-driven TEMs (i.e., $\eta_e = 0$) shown in Fig. 4(c) of Ref. [2], highlighting the impact of the exact field operator for $\eta_e \sim 1$. This η_e dependence is corroborated by the broad parameter scans of the TEM growth rates in Fig. 3. Finally, this Letter presents the material impact of the exact collision operator on MTMs in the collisional JET pedestal. Overall, the sensitivity to the exact field-particle terms is greatest for instabilities driven by the electron temperature gradient, including TEMs and MTMs. We speculate that the reason field operator corrections matter for a finite η_e in both instability types is that model field operators are in effect a truncation of the Hermite-Laguerre moment energy expansion of the distribution [19], while η_e enters the gyrokinetic equation with an energy weighting, i.e., through the coefficient $1 + \eta_e(E/T_e - 3/2)$ of the density gradient, where E is the particle energy. Accordingly, the temperature gradient drive affects higher energy moments of the distribution, which are neglected in model field operators.

Future work is needed to evaluate impact of the exact particle collisions on global confinement for specific fusion experiments and scenarios. The fusion power is proportional to the square of the plasma pressure, and depends sensitively on the plasma density and temperature radial profiles. Relatively small changes in local density and temperature gradients in or near the edge can produce a significant integral impact on plasma profiles in the core region, where the majority of fusion reactions take place. The exact treatment of collisions could be important in negative triangularity plasmas where temperature-gradient-driven TEM turbulence dominates [31], could impact the isotope effect due to TEM turbulence [32], and could be useful for magnetized space and astrophysical plasmas such as the solar wind, where gyrokinetic simulations with the same code suggest collisional dissipation plays an important role in the kinetic Alfvénic turbulence [33]. Our ongoing work will improve the computational efficiency of the exact operator in order to perform more high-quality nonlinear simulations using a velocity-space spectral method [34,35].

Acknowledgments. We thank Dr. T. Görler, Dr. D. Told, and Dr. F. Jenko for useful discussions and support of the GENE code. The Sugama collision model was implemented in GENE by Dr. P. Crandall as part of his Ph.D. thesis. Simulations utilized resources of the National Energy Research Scientific Computing Center, operated under US DOE Contract No. DE-AC02-05CH11231. This work is supported by US DOE Contract No. DE-FC02-08ER54966 and the SciDAC Partnership for Multiscale Gyrokinetic Turbulence, US DOE Contract No. DE-SC0018429 (Subaward No. UTA18-000276).

[1] E. A. Frieman and L. Chen, Phys. Fluids **25**, 502 (1982).
[2] Q. Pan, D. Ernst, and P. Crandall, Phys. Plasmas **27**, 042307 (2020).
[3] H. Sugama, T.-H. Watanabe, and M. Nunami, Phys. Plasmas **16**, 112503 (2009).
[4] M. Nakata, M. Nunami, T.-H. Watanabe, and H. Sugama, Comput. Phys. Commun. **197**, 61 (2015).
[5] E. A. Belli and J. Candy, Plasma Phys. Controlled Fusion **59**, 045005 (2017).
[6] P. Crandall, D. Jarema, H. Doerk, Q. Pan, G. Merlo, T. Görler, A. Bañón Navarro, D. Told, M. Maurer, and F. Jenko, Comput. Phys. Commun. **255**, 107360 (2020).
[7] I. G. Abel, M. Barnes, S. C. Cowley, W. Dorland, and A. A. Schekochihin, Phys. Plasmas **15**, 122509 (2008).
[8] P. J. Catto and D. R. Ernst, Plasma Phys. Controlled Fusion **51**, 062001 (2009).
[9] Q. Pan and D. R. Ernst, Phys. Rev. E **99**, 023201 (2019).
[10] F. Jenko, W. Dorland, M. Kotschenreuther, and B. N. Rogers, Phys. Plasmas **7**, 1904 (2000).
[11] https://genecode.org.
[12] B. Li and D. R. Ernst, Phys. Rev. Lett. **106**, 195002 (2011).
[13] E. S. Yoon and C. S. Chang, Phys. Plasmas **21**, 032503 (2014).
[14] E. A. Belli and J. Candy, Plasma Phys. Controlled Fusion **54**, 015015 (2012).
[15] D. R. Ernst *et al.*, Phys. Plasmas **23**, 056112 (2016).
[16] A. M. Dimits *et al.*, Phys. Plasmas **7**, 969 (2000).
[17] D. Ernst *et al.*, Phys. Plasmas **11**, 2637 (2004).
[18] D. R. Ernst *et al.*, in Proceedings of the 21st International Atomic Energy Agency Fusion Energy Conference, 2006, IAEA-CN-149/TH/1-3: http://www-pub.iaea.org/MTCD/Meetings/FEC2006/th_1-3.pdf.
[19] S. P. Hirshman and D. J. Sigmar, Phys. Fluids **19**, 1532 (1976).
[20] M. Oberparleiter, H. Nordman, G. Verdoolaege, and F. Jenko, J. Phys.: Conf. Ser. **775**, 012009 (2016).
[21] F. L. Hinton and M. N. Rosenbluth, Plasma Phys. Controlled Fusion **41**, A653 (1999).
[22] H. Doerk, F. Jenko, M. J. Pueschel, and D. R. Hatch, Phys. Rev. Lett. **106**, 155003 (2011).
[23] W. Guttenfelder *et al.*, Phys. Rev. Lett. **106**, 155004 (2011).
[24] D. Dickinson *et al.*, Plasma Phys. Controlled Fusion **55**, 074006 (2013).

[25] D. Hatch *et al.*, Nucl. Fusion **56**, 104003 (2016).
[26] X. Jian, C. Holland, J. Candy, E. Belli, V. Chan, A. M. Garofalo, and S. Ding, Phys. Rev. Lett. **123**, 225002 (2019).
[27] M. Leyland *et al.*, Nucl. Fusion **55**, 013019 (2014).
[28] X. Q. Xu and M. N. Rosenbluth, Phys. Fluids B **3**, 627 (1991).
[29] T. Xie, M. J. Pueschel, and D. R. Hatch, Phys. Plasmas **27**, 082306 (2020).
[30] D. R. Hatch *et al.*, Nucl. Fusion **61**, 036015 (2021).
[31] A. Marinoni *et al.*, Phys. Plasmas **26**, 042515 (2019).
[32] D. R. Ernst, New mechanisms for improved confinement with isotopic mass, in International Sherwood Fusion Theory Conference, April 15-17, Princeton, New Jersey, 2019 (unpublished); http://www.sherwoodtheory.org/sw2019/uploads/273/ernst_sherwood19_abstract.pdf.
[33] D. Told, F. Jenko, J. M. TenBarge, G. G. Howes, and G. W. Hammett, Phys. Rev. Lett. **115**, 025003 (2015).
[34] M. Landreman and D. R. Ernst, J. Comput. Phys. **243**, 130 (2013).
[35] A. Pataki and L. Greengard, J. Comput. Phys. **230**, 7840 (2011).